Delft University of Technology

Ruthenium particle size and cesium promotion effects in Fischer-Tropsch synthesis over high-surface-area graphite supported catalysts

Eslava, José L.; Sun, Xiaohui; Gascon, Jorge; Kapteijn, Freek; Rodríguez-Ramos, Inmaculada

Important note
To cite this publication, please use the final published version (if applicable).
Please check the document version above.

ROYAL SOCIETY OF CHEMISTRY

Journal Name

ARTICLE

Ruthenium particle size and cesium promotion effects in Fischer-Tropsch synthesis over high-surface-area graphite supported catalysts

José L. Eslava[a], Xiaohui Sun[b], Jorge Gascon*[b], Freek Kapteijn[b] and Inmaculada Rodríguez-Ramos*[a]

The effect of ruthenium particle size on Fischer-Tropsch synthesis (FTS) has been studied at 513 K, H_2/CO = 2 and 15 bar. Supported Ru catalysts with particle sizes ranging from 1.7 to 12 nm were prepared by using different Ru loadings and two different high surface area graphite (HSAG) supports to minimize the metal-support interaction. In addition, the effect of promotion with Cs is also evaluated. Microcalorimetric characterization during CO adsorption and XPS reveal a clear interaction between Ru and Cs. The FTS with Ru-based catalysts is, independent of the presence of promoter, highly structure-sensitive when the Ru particle size is under 7 nm. In this range the turnover frequency (TOF) for CO conversion increases with particle size, reaching a near constant value for Ru particles larger than 7 nm. Cs promoted catalysts display lower TOF values than the corresponding unpromoted samples. This somewhat reduced activity is attributed to the stronger CO adsorption on Cs promoted catalysts, as demonstrated by CO adsorption microcalorimetry. Product selectivity depends also on Ru particle size. Selectivity to C_{5+} hydrocarbons increases with increasing Ru particle size. For Cs-promoted catalysts, the olefin to paraffin ratio in the C_2-C_4 hydrocarbons range is independent of the Ru particle size, whereas it decreases for the unpromoted catalysts, showing the prevailing influence of the promoter.

Introduction

Fischer-Tropsch synthesis (FTS) is a key technology which allows the transformation of synthesis gas, a mixture of CO and H_2 from various non-petroleum carbon resources such as natural gas, coal and biomass, into clean hydrocarbon fuels as well as valuable chemicals. Iron and cobalt are the usual metals for FTS. Ruthenium catalysts, notwithstanding higher price, possess some unique features in FT synthesis (highest activity and prominent chain-growth probability), that render them unique for fundamental research.[1-3] In addition, Ru catalysts can be employed under higher partial pressures of water and other oxygenates, opening the door for a perspective application of these catalysts in the conversion of syngas produced from biomass. It is known that FT catalysts usually require promoters such as alkali metals, noble metals or transition metal oxides to attain the optimal catalytic performance.[2] Modification with alkali metal ions increases both the activity and selectivity for high molecular weight hydrocarbons and favors the formation of olefins.[4,5] This behavior could be explained by the basicity of the alkali promoter, which is proposed to raise the CO dissociative adsorption rate, increasing the surface coverage of dissociated CO and lowering the hydrogen coverage. In this sense, the alkali promoter shifts the hydrocarbon selectivity towards longer chain hydrocarbons and olefin products.[6] Furthermore, it has been reported that such alkali elements (Na, K or Cs) are electronic promoters that transfer part of their electron density to Ru even in its oxidized state, which strengthens the CO-metal interaction whereas weakening the C-O bond.[4,7-9] Recently, some experimental evidences of the partial reduction of Cs in Cs-Ru/C catalysts during temperature-programmed reduction have been provided by X-ray absorption spectroscopy.[10]

Almost all FT catalysts use a support that has a significant effect on the reducibility, activity and selectivity of the active phase and promoters.[11,12] Selection of a support with a proper interaction with the active phase (or metal precursor) is of prime importance because of the balance between the reducibility and the dispersion of the active phase that defines FTS performance. Supports such as alumina,[13,14] silica,[15,16] titania[17] and carbon materials[10,18-22] have been reported by many groups. Among them, carbon materials are considered to be more inert than the conventional oxide materials. This allows the study of the intrinsic properties of the ruthenium particles, in contrast to oxidic supports where poorly reducible mixed oxides may interfere during catalyst synthesis or FT catalysis.

Fischer-Tropsch synthesis is recognized as a structure sensitive reaction, which means that the surface-specific activity

a. Instituto de Catálisis y Petroleoquímica, CSIC, C/Marie Curie 2, 28049 Madrid, Spain.
   E-mail: irodriguez@icp.csic.es
b. Catalysis Engineering, Dept. Chemical Engineering, Delft University of Technology, Van der Maasweg 9, 2629 HZ Delft, The Netherlands.
   E-mail: j.gascon@tudelft.nl

(TurnOver Frequency, TOF) is a function of the metal particle size.[18,19,23,24] The effect of metal particle size on the catalytic performance has been extensively studied by several authors for cobalt,[25-27] with earliest contributions from Bartholomew[28] and Yermakov,[29] and for iron.[24,30,31] However, in the case of ruthenium, the number of research studies is certainly more limited. During the 80s, a few studies pointed out the increase in TOF for CO hydrogenation with increasing the size of Ru supported on alumina (or decreasing the metal dispersion from 0.78 to 0.16).[32,33] It was also shown that the TOFs over Ru catalysts loaded on metal oxides such as SiO_2, Al_2O_3 and TiO_2 were independent of the dispersion of Ru in the range studied (0.0009–0.60).[34] Recently, Kang et al.[19,35] studied the size-effects for FT synthesis catalyzed by Ru nanoparticles loaded on carbon nanotubes. They reported that the TOF increased significantly with the mean size of Ru up to approximately 6 nm and then decreased only slightly with further size increases. The C≥5 selectivity also underwent a gradual increase with increasing the mean Ru particle size from 2.3 to 6.3 nm. Carballo et al.[36] investigated the size effect of Ru particles supported on γ-Al_2O_3 and found that the FT synthesis with Ru/γ-Al_2O_3 catalysts is a strongly structure-sensitive reaction when the size of Ru particles was smaller than 10 nm. Theoretical understanding of the origin of the effect of metal particle size on reaction rates of a given reaction has been tackled by Van Santen et al.[23,37] They stated that the CO activation in the FT reaction needs a reaction center with a particular configuration of several metal atoms and step-edge sites, which geometrically may not be present below a particle size of 2 nm.

As the support material may mask the metal particle size effects, research focused on intrinsic ruthenium particle size effects may be advantageously performed using an inert support material, such as graphitic carbon. To clarify the effect of Ru particle size on catalytic performance in FT synthesis, we have prepared Ru catalysts supported on high surface area graphite (HSAG) varying the size of Ru particles from 1.7 to 12 nm by using two HSAGs with different surface area (100 and 400 m^2/g) and various Ru loadings. In addition we have explored the effect of alkali promotion (Cs) on these systems.

Experimental section

Catalyst preparation

Two different high surface area graphites from TIMCAL (G100, SBET = 100 $m^2 \cdot g^{-1}$ and G400, S_{BET} = 400 $m^2 \cdot g^{-1}$) were used as catalyst supports. The monometallic ruthenium catalysts were prepared by incipient wetness impregnation using water:ethanol (1:1) solutions of ruthenium chloride hydrate ($RuCl_3 \cdot xH_2O$ from Aldrich) in the adequate concentration to incorporate 20, 10 and 5 wt% Ru to the support. After impregnation, the catalysts were kept at room temperature overnight and later heated at 393 K during 24 h. The ruthenium and cesium bimetallic catalysts were prepared by incipient wetness co-impregnation with water:ethanol (1:1) solutions of ruthenium chloride and cesium choride with

adequate concentrations to obtain a Ru/Cs ratio of 20. The loading of ruthenium and cesium in the catalysts was determined by total reflection X-ray fluorescence (TRXF). Table 1 summarizes the chemical composition of the prepared catalysts.

Table 1. Ruthenium and cesium loading for all catalysts.

Catalyst	Ru (wt%)	Cs (wt%)
20Ru/G100	17.3	-
20Ru1Cs/G100	16.6	1.00
10Ru/G100	9.3	-
10Ru0.5Cs/G100	9.4	0.50
5Ru/G100	5.1	-
5Ru0.25Cs/G100	4.9	0.25
20Ru/G400	16.6	-
20Ru1Cs/G400	16.8	1.00
4Ru/G400	3.6	-

Catalyst Characterization

Temperature-programmed reduction (TPR) measurements were carried out in a U-shaped quartz microreactor using 100 mg of sample in a continuous flow of 20 ml/min of a H_2/Ar gas mixture (5% H_2). The temperature was increased from room temperature to 1273 K at 5 K/min. After H_2O removal the H_2 consumption was monitored by a TCD and the desorbed products were analysed by a mass spectrometer.

The specific surface area of the fresh catalysts was measured by N_2 adsorption isotherms at 77 K using a Micromeritics ASAP 2010 volumetric system. Prior to N_2 adsorption, the catalysts were degassed at 423 K overnight. The BET model was used to obtain the specific surface area of samples.

CO uptake and the evolution of CO adsorption heat were recorded in a Tian Calvet heat-flow microcalorimeter (Setaram C-80 II) isothermally operated at 331 K and connected to a glass vacuum-dosing apparatus. The metal surface was titrated by treating the samples with successive pulses of CO, following the experimental procedure described in detail elsewhere.[38] The catalysts were first activated by reduction in H_2 flow (60 ml/min) at 673 K during 2 h. Metal dispersion (D_{CO}) was calculated assuming a molar stoichiometry Ru/CO = 1/1, from the total CO uptake at the monolayer considered to be attained when the evolved heat falls below the physisorption threshold (40 kJ/mol). The mean metal crystallite size was calculated from the dispersion values assuming the spherical model, dco (nm) = 1.32/D_{CO}.[39]

X-ray photoelectron spectra of the catalysts were recorded with an electron spectroscopy system SPECS GmbH with UHV system, energy analyzer PHOIBOS 150 9MCD using a monochromatic X-ray source (with double anode Al/Ag), source of electrons for charge compensation, ultraviolet photon source, ion source and sample pretreatment chamber (HPC). Each sample was pressed into a small pellet of 10 mm diameter, placed in the sample holder and degassed in the chamber for 24 h to achieve a dynamic vacuum below 10^{-10} mbar before analysis. The catalysts were first activated by reduction in H_2 flow (70 ml/min) at 673 K during 1 h in the

sample pretreatment chamber. The spectral data for each sample were analyzed using CASA XPS software. The C1s peak at 284.6 eV was used as an internal standard. The equipment error in the energy determinations is less than 0.01 eV. The relative concentrations and atomic ratios were determined from the integrated intensities of photoelectron lines corrected for the corresponding atomic sensitivity factor.

The X-ray diffraction (XRD) patterns were registered in a Bruker D8 Advance diffractometer equipped with a Vantec position sensitive detector and graphite monochromator. Measurements were executed at room temperature, using monochromatic Co Kα radiation (λ = 0.179026 nm) in the 2θ region between 10° and 100° with a step size of 0.038°.

Transmission electron microscopy (TEM) measurements of the used catalysts were undertaken using a JEOL JEM-2100 field emission gun electron microscope operated at 200 kV. The samples were ground and ultrasonically suspended in hexane before deposition over a copper grid with carbon coated layers. Ru particle diameter (d_{TEM}) was calculated based on a minimum of 350 particles (Table 2) using the following equation:[40]

$$d_{TEM} = \frac{\sum_i n_i d_i^3}{\sum_i n_i d_i^2} \qquad (1)$$

Where n_i is the number of particles with diameter d_i.

Catalytic Measurements

FT experiments were carried out in a six-flow fixed-bed microreactor setup which permitted running six reactions in parallel under identical feed composition, temperature, and conditions of separation/analysis following the experimental procedure described in detail elsewhere.[41]

For FTS, 0.5 g of fresh catalyst was fixed in the reactor and diluted with SiC of the same particle size (100-212 μm). Samples were first activated in situ by 80 cm³$_{STP}$ min^{-1} of H$_2$ at 673 K for 12 h at atmospheric pressure followed by cooling down to 453 K under H$_2$ flow. Then the pressure was increased to 15 bar and CO was gradually introduced to the feed stream at 453 K in order to reach its final concentration (H$_2$/CO = 2) in 1 h. Afterwards, the reactor was heated to the process temperature (513 K). A rate of 2 K min^{-1} was applied for all the heating/cooling steps. A controlled nitrogen flow was added after each reactor that served as an internal standard for the analysis.[42,43]

After 75 or 45 h on-stream a pseudo-steady-state catalytic behavior was achieved and selectivity data were collected. CO conversion, carbon selectivity, molar fraction of each product were defined by Eqs. (2)-(4), where X_{CO} stands for CO conversion, F indicates the molar flow, S is the carbon selectivity towards a product with n carbon atoms and Y is the molar fraction of a hydrocarbon C$_n$.

$$X_{CO} = \frac{F_{in,CO} - F_{out,CO}}{F_{in,CO}} \; x \; 100 \qquad (2)$$

$$S_{Cn} = \frac{nF_{Cn}}{F_{CO_2} + \sum_{n=1}^{N} nF_{Cn}} \; x \; 100 \qquad (3)$$

$$Y_{Cn} = \frac{F_{Cn}}{\sum_{n=1}^{N} F_{Cn}} \qquad (4)$$

Carbon balances were all better than 95%. Reproducibility of the experiments was within ±5%. The catalytic activities expressed as μmol CO converted to hydrocarbons per gram of ruthenium per second were calculated from the equation:

$$A = \frac{C \cdot F_{CO}}{100 \, W_{Ru}} \left(\frac{\mu mol}{g_{Ru} s} \right)$$

where C is the CO converted percentage, F is the CO flow rate (μmol/s) through the reactor, and W_M is the weight (g) of metal in the catalyst. Also the activity per mol of surface metal sites per second or turnover frequency (TOF) was determined following the expression:

$$TOF = \frac{A}{N_{surf}} (s^{-1})$$

where N_{surf} is the μmol of surface metal sites per gram of metal in the reactor.

Results and discussion

Catalysts Characterization

Figure 1 shows the TPR profiles of the non-promoted and Cs-promoted ruthenium samples. All catalysts show two overlapping peaks of hydrogen consumption at around 400 K, the envelope being centered in the second peak, that can be assigned to the reduction of Ru (III) to Ru(0) species.[44,45] At temperatures above 700 K hydrogen is also consumed for all catalysts due to the partial gasification of the carbon support around metallic particles to give CH$_4$, as previously reported for other carbon supported Ru catalysts.[46] 20Ru and 20Ru1Cs/G400 catalysts show the Ru reduction peak with a maximum at around 427 K whereas catalysts of Ru, Ru-Cs/G100 series exhibit the main peak at temperatures that range from 412 up to 450 K. The variation in reduction temperature is related with the different particle size of Ru in the catalyst as will be later discussed. Larger Ru particles are reduced at higher temperature than small Ru particles due to the absence of interaction of the metal with the graphite support. From the TPR characterization, it can be assured that all the catalysts are completely reduced during the treatment in hydrogen at 673 K.
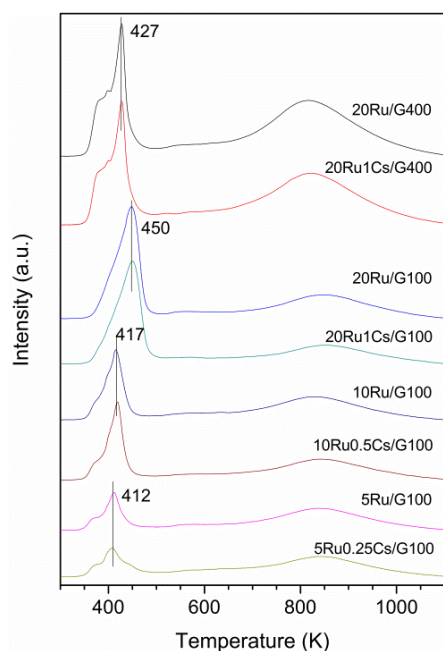
Figure 1. Hydrogen consumption profiles during temperature programmed reduction for the Ru and Ru-Cs catalysts (5 K/min).

Diffraction patterns of the Ru catalysts reduced at 673 K are displayed in Figure 2. The sharp reflections at 30.6^o and 65° are characteristic of the graphite structure and become sharper when the graphitic character of the support increases. Reflections at 2θ = 45°, 49°, 51°, 70° and 85° (grey triangles in Figure 2) characteristic for metallic ruthenium are also observed in the Ru/G and Ru-Cs/G catalysts. These reflections have low intensities and are quite wide, indicating a high dispersion of the ruthenium in the catalysts. The average particle sizes of ruthenium crystallites, calculated from the most intense reflection at 2θ = 51° using the Scherrer equation, are shown in Table 2. 20Ru1Cs/G100 and 20Ru/G100 catalysts have the largest particle size followed by 10Ru0.5Cs/G100 and 10Ru/G100 catalysts. For the other catalysts no reflections of metallic ruthenium were observed indicating that the particle size values are below to the experimental detection limit for the XRD technique (4.5 nm).
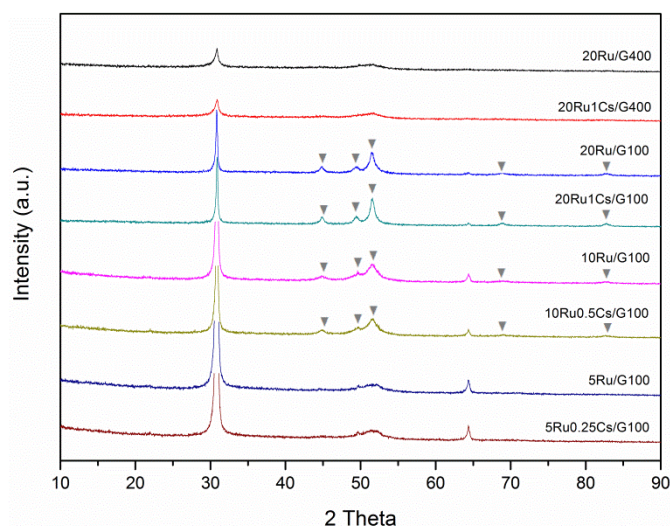
Figure 2. XRD pattern after reduction in H$_2$ at 673 K for Ru and Ru-Cs catalysts. (▼) Reflections from Ru(0) phase.

Table 2 also summarizes the CO uptakes and the average metal particle sizes obtained from both CO chemisorption and TEM measurements for the non-promoted and Cs promoted ruthenium catalysts. Particle sizes determined by TEM are smaller than those obtained by CO chemisorption independently of the catalyst composition. However, the TEM-values are very similar to those determined from XRD (when data are available). Residual chloride species anchored on Ru metal particles or close to them may block adsorption sites for CO molecules. It is considered that some chloride species may remain on the catalyst surfaces even upon the reduction treatment applied at 673 K.[47,48] Moreover, though the CO can chemisorb in various forms on Ru nanoparticles, in this work a Ru-CO stoichiometry 1:1 is assumed for metal dispersion calculation. But the presence of adsorbed CO in bridging configuration on two Ru atoms is possible and this would be reflected in larger average particle sizes of ruthenium.

TEM analysis suggests that addition of Cs to the ruthenium catalyst slightly increases the ruthenium metal particle size compared to the unpromoted catalyst. By contrast, CO chemisorption shows the opposite effect, attributed to the presence of the promoter which increases the amount of CO molecules adsorbed on the catalyst surface. This suggests that the CO adsorption mode is changed on Ru atoms adjacent to Cs ions from bridged toward linear adsorption.

Table 2. Textural properties of the ruthenium and cesium promoted catalysts reduced in hydrogen at 400°C for 2 h.

Catalyst	CO uptake (μmol/g$_{Ru}$)	d_{CO} (nm)	d_{XRD} (nm)	d_{TEM} (nm)[++]
20Ru/G100	65	33.2	17.2	12.0 ± 2.8
20Ru1Cs/G100	83	26.4	18.4	12.7 ± 2.9
10Ru/G100	67	18.1	8.4	7.1 ± 1.6
10Ru0.5Cs/G100	78	15.6	9.0	7.5 ± 1.4
5Ru/G100	58	11.5	*	3.4 ± 0.9
5Ru0.25Cs/G100	61	10.5	*	4.2 ± 1.0
20Ru/G400	150	14.6	*	3.6 ± 0.9
20Ru1Cs/G400	202	10.8	*	4.2 ± 1.0
4Ru/G400	98	4.5	*	1.7 ± 0.4

* Below technique detection limit (< 4.5 nm)

[++] Standard deviation of the set of values used to determine the average particle size is included for each sample.

Representative TEM images of the catalysts and histograms with particle size distributions are shown in Figures 3 and 4. Comparison of catalysts with the same metal loading but with increasing surface area of support reveals that the average particle size of ruthenium decreases by a factor of four, in line with the increase in available surface area (see Table 2 and also compare the histograms in Figures 3a and 3d). Furthermore, the catalyst supported on graphite with lower surface area, 20Ru/G100, presents a Ru particle size distribution wider than that on the graphite with higher surface area, 20Ru/G400. Similar features are observed for catalysts with the same support when ruthenium metal loading is decreased: the average particle size of ruthenium decreases from 12 to 3.4 nm and the particle size distribution becomes narrower (see Table 2 and Figures 3a, 3b and 3c). Next to a slight increase, the particle size distribution broadens for all catalysts after Cs addition, especially for 20Ru1Cs/G100 and 10Ru0.5Cs/G100 catalysts where the frequency of particles larger than 16 or 7 nanometers, respectively, is significantly incremented (Figure 4).
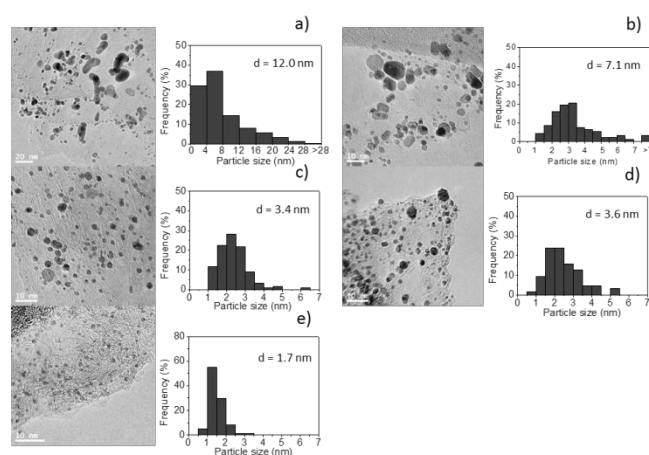
Figure 3. Particle size distribution and TEM images of reduced Ru catalysts. (a) 20Ru/G100, (b) 10Ru/G100, (c) 5Ru/G100 (d) 20Ru/G400, (e), 4Ru/G400.
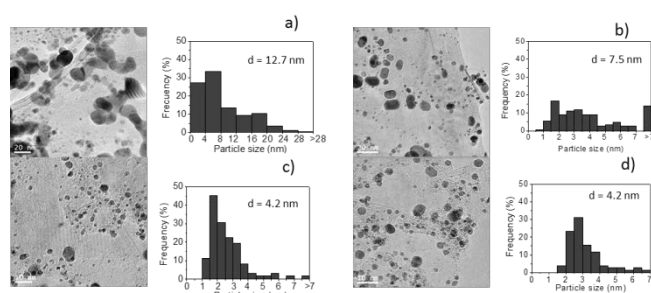
Figure 4. Particle size distribution and TEM images of reduced Ru-Cs catalysts (a) 20Ru1Cs/G100, (b) 10Ru0.5Cs/G100, (c) 5Ru0.25Cs/G100, (d) 20Ru1Cs/G400.

Information about the strength and energetic distribution of the surface adsorption sites on the catalysts was obtained from the microcalorimetric profiles of CO adsorption. Figure 5 shows the differential enthalpies of CO adsorption (Q_{diff}) as a function of surface coverage for the 10Ru/G100, 10Ru0.5Cs/G100, 5Ru/G100 and 5Ru0.25Cs/G100 catalysts reduced at 673 K in hydrogen for 2 h. Adsorption heat values and shapes of microcalorimetric profiles are different, depending on the metal content and presence of promoter. The profiles for 5Ru/G100 and 5Ru0.25Cs/G100 catalysts (Figure 5b) exhibit a high initial adsorption heat of 128 kJ/mol. This high value is typical of highly energetic active sites usually associated with small ruthenium nanoparticles, with preferentially populated edges, corners and other metallic low coordinated Ru-sites. This initial adsorption heat quickly decreases to reach a constant value of 95 and 105 kJ/mol (5Ru/G100 and 5Ru0.25Cs/G100, respectively) for surface coverages from 0.1-0.2 to 0.8 and finally drops down to 40 kJ/mol (physisorption values). Beyond coverage ranges of 0.8 the intensity of the dipole-dipole interactions among CO molecules adsorbed on Ru faces increases weakening the metal-CO bond. It is important to note that the CO adsorption heats on Cs promoted ruthenium catalyst are higher than those of the unpromoted Ru catalyst, for the surface coverage range from 0.1 to 0.8 (Figure 5b). According to certain authors,[7,8,49] cesium is believed to act as electronic promoter donating part of its electron density to Ru even in its oxidized form. A partial reduction would promote more efficient charge transfer to Ru, as was shown in previous works.[10] Such electronic transfer would produce a strengthening in the π component of the Ru-CO bond (by larger π back-donation from the metal atoms to antibonding molecular orbitals of the CO molecule). Due to the synergetic character of the two contributions (σ and π) to the metal-CO molecule bond the overall metal-CO bond is strengthened and higher CO adsorption heats would be obtained.[22]

This electronic effect is also observed comparing the 10Ru/G100 and 10Ru0.5Cs/G100 catalysts (Figure 5a). Similarly, CO adsorption heats on Cs promoted ruthenium catalyst are higher than those of the non-promoted Ru catalyst due to the cesium promoter effect. In this case, a plateau with constant adsorption heat values from 0.05 to 0.3 coverage, without highly strong surface sites at very low coverage (lower than 0.2), and further a slow decrease up to a fractional coverage of 0.8 is observed. This finding reveals the absence of

highly energetic active sites such as, edges, corners or other metallic (Ru) low coordinated sites because in these samples ruthenium particles sizes are greater, as discussed above.
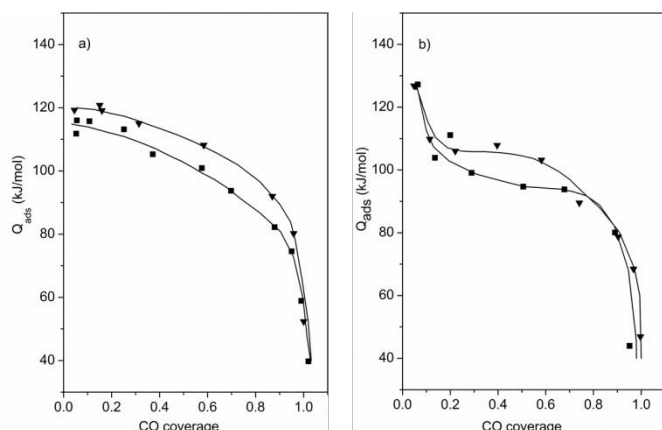
Figure 5. Differential heats of CO adsorption at 331 K as a function of surface coverage for: (a) (■) 10Ru/G100, (▼) 10Ru0.5Cs/G100 catalysts and (b) (■) 5Ru/G100 and (▼) 5Ru0.25Cs/G100 catalysts.

Comparison of 10Ru/G100 and 5Ru/G100 also reveals that the increase in Ru loading results in higher heats of CO adsorption over the coverage range from 0.1 to 0.7. If the two Cs promoted catalysts are compared between each other, a similar trend is observed. The large proportion of surface sites with higher adsorption heats shown by catalysts with 10 wt% Ru loading may be attributed to an increase of the electron density of the Ru sites due to the presence in these samples of larger metal particles (see Table 2).

Surface composition and electronic state of Ru in 10Ru and 10Ru0.5Cs/G100 catalysts was investigated by XPS. The XPS spectra in the region of Ru $3d_{5/2}$ peak are shown in figure 6.
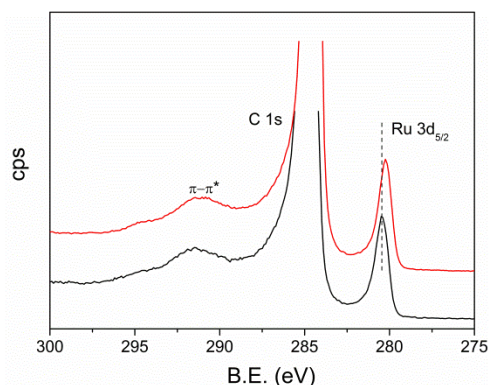
Figure 6. XPS spectra in the Ru $3d_{5/2}$ region for 10Ru/G100 (black line) and 10Ru0.5Cs/G100 (red line) catalysts after in-situ reduction treatment at 673 K. The C 1s peak of graphite masks the $3d_{3/2}$ component of the Ru 3d doublet.

Table 3. XPS analysis

Sample	B.E. Ru $3d_{5/2}$ (eV)	XPS ratios	
		Ru/C	Cs/C
10Ru/G100	280.45	0.011	-
10Ru0.5Cs/G100	280.24	0.011	0.001

Data in Table 3 show that the binding energy of Ru $3d_{5/2}$ was of 280.45 and 280.24 eV for 10Ru and 10Ru0.5Cs/G10, respectively, which is assigned in the literature to reduced forms of ruthenium.[50] The binding energy of Ru $3d_{5/2}$ on the Cs promoted catalyst shifts 0.21 eV towards lower energy values. This shift to lower binding energy suggests an electron enrichment of the surface Ru atoms. The increase in electron density of ruthenium atoms may be attributed in a first stage to the slight increase in Ru particle size observed in the promoted catalyst with respect to the non-promoted (see TEM and XRD data in Table 2) since electron density of metal particles increases with the growing particles size.[51-53] But the existence of an electronic interaction between Ru and Cs with electron transfer from Cs to Ru can definitively lead to an enhanced electron density of Ru atoms as already postulated from the CO chemisorption measurements.

Fischer-Tropsch Synthesis

Promoted and unpromoted Ru catalysts were tested under FTS conditions at 15 bar to assess the effect of ruthenium particle size on catalytic performance. Equal amount of catalyst (0.5 g) was used in all the experiments. Figure 7 shows the evolution of CO conversion during 80 h on stream and reveals that after 30 h the reaction reaches steady state conditions. Conversions decrease as foreseen for decreasing Ru loadings, but also on the same loading for lower Ru particle sizes.
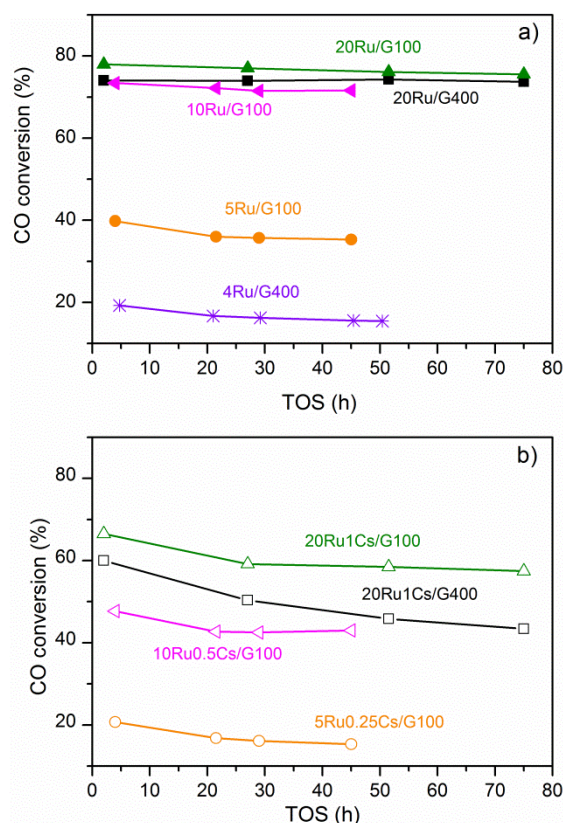
Figure 7. Time-on-stream (TOS) evolution of CO conversion during FTS at 513 K, 15 bar, $H_2/CO = 2$ and GHSV = 6.1 m^3_{STP} kg^{-1} h^{-1}. (a) non-promoted and (b) Cs promoted catalysts.

Table 4 lists catalytic activity and product selectivity under steady state conditions for all the catalysts. The O/P values calculated from the ratio of olefin to paraffin in the range of C_2-C_4 hydrocarbons and hydrocarbon chain-growth probabilities (α) from Anderson-Schulz-Flory (ASF) plots using a linear regression over carbon numbers three to twenty are also included in Table 4.

Table 4. Catalytic performance in the Fischer–Tropsch synthesis of Ru and Ru-Cs catalysts reduced at 673 K[a].

Catalyst	Activity (μmol/ g_{Ru} s)	CO Conv. (%)	CO_2 Select. (%)	Product distribution			$α^d$	O/P[e]
				CH_4	C_2-C_4	C_{5+}		
20Ru/G100[b]	115.8	76	0.2	18	11	71	0.85	0.48
20Ru1Cs/G100[b]	86.5	57	0.8	4	5	91	0.88	2.17
10Ru/G100[c]	191.4	72	0.1	22	13	65	0.84	0.79
10Ru0.5Cs/G100[c]	113.7	43	0.2	7	7	86	0.86	2.18
5Ru/G100[c]	170.5	35	0.3	28	18	54	0.78	0.98
5Ru0.25Cs/G100[c]	77.1	15	0.0	21	15	64	0.80	2.24
20Ru/G400[b]	112.1	74	0.4	31	23	46	0.73	1.09
20Ru1Cs/G400[b]	64.0	43	0.0	21	11	68	0.81	2.10
4Ru/G400	106.6	15	0.0	49	19	32	0.70	1.13

[a] Reaction conditions: CO/H_2 (1/2, flow rate = 50 ml/min), pressure of 15 bar, temperature of 513 K, catalyst (0.5 g).

[b] 75 h time on stream.

[c] 45 h time on stream.

[d] The α value was calculated using Anderson–Schulz-Flory (ASF) distribution in the hydrocarbon range of C_3-C_{20}.

[e] The O/P value was calculated from the ratio of olefin to paraffin in the range of C_2-C_4 hydrocarbons

Independently of the support, loading and ruthenium particle size, the addition of the promoter implies a decrease in the catalytic activity, an enhancement of light olefin production (higher O/P ratio) and higher selectivity toward C_{5+} hydrocarbons (increased α) compared to its non-promoted counterparts. These results agree with previous X-ray absorption spectroscopy results[10] where we demonstrate the close interaction between Ru and Cs supported on high surface area graphite under FT reaction atmosphere and its effects in the catalytic performance. Similarly, the above XPS experiments revealed the electronic interaction between Ru and Cs, which is further supported by the stronger CO adsorption measured by microcalorimetry. According to the FT mechanism, long-chain-hydrocarbon formation involves the polymerization of CH_x species, formed from CO dissociation and subsequent C hydrogenation,[54] following the Anderson-Schulz-Flory distribution.[2] The termination of the chain can occur by H addition or by β-elimination resulting in paraffins or olefins, respectively. So on the promoted catalysts, the higher population of adsorbed dissociative CO and formation of CH_x species on the surface likely hinder the hydrogen adsorption favoring the chain growth by C-C coupling and the olefin formation. Concurrently, the higher population of C_1 adsorbed species, as already reported,[55] self-blocks the active sites for

further CO dissociation as a consequence the overall rate of the reaction becomes slower.

To gain further information about the effect of Ru particle size on catalytic activity, the turnover frequency (TOF) for CO conversion over the unpromoted and promoted Ru catalysts with different sizes of Ru particles is compared in Figure 8. The TOF values were calculated based on the Ru dispersion from TEM measurements.
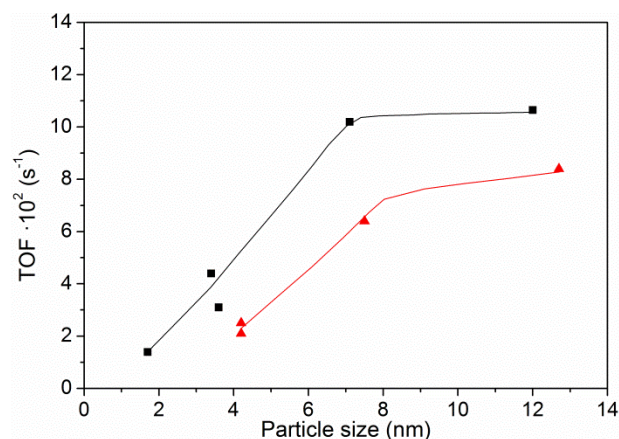

Figure 8. The influence of ruthenium particle size on the TOF for (■) non-promoted and (▲) Cs-promoted catalysts

The TOF is rather constant with a value of around 10^{-1} s^{-1} for non-promoted ruthenium particles above 7 nm and up to 12 nm. For smaller particle sizes, the TOF decreases down to a value of 10^{-2} s^{-1} for the 4Ru/G400 catalyst. In the case of Cs-promoted catalysts the TOF follows the same trend as a function of the Ru particle size, although the TOF-values are decreased by a factor which seems to be independent of metal particle size. In terms of catalytic activity the effectiveness of promotion is similar for small and large particles. Recent studies reported that the critical Ru-particle size below which the CO consumption rate becomes structure sensitive is in the 6-10 nm.[19,36] This structure-sensitive behavior has been attributed to the decreasing stability of step-edge sites on the surface of smaller particles. These sites, which consist of an ensemble of five metal atoms located at the step edges of large particles and referred to as B5 sites, have been proposed to be essential for low-barrier CO dissociation.[23,37,54] In this line, our data support the assumption that a minimum size of the nanoparticles is required to sustain surface sites needed for facile CO dissociation.

Regarding product selectivities, Figure 9 shows the changes in selectivity towards different hydrocarbons with the average size of Ru particles for unpromoted (Figure 9.a) and promoted (Figure 9.b) catalysts. Selectivity differences between catalysts should be considered with care in the case of large conversion differences between catalysts in view of possible different extents of secondary reactions. In our case, the CO conversion over the non-promoted 5Ru/G100 and 20Ru/G400 catalysts with very similar Ru particle size, 3.4 and 3.6 nm, respectively (see Figure 3 and Table 2), varied from 35 to 74% (Table 4), whereas the selectivity towards the different products only

slightly changed. A similar picture can be described for the promoted 5Ru0.25Cs/G100 and 20Ru1Cs/G400 catalysts (both with mean Ru particle size of 4.2 nm), which gave similar product distributions for CO conversions of 15 and 43%, respectively. Therefore, under the FTS reaction conditions used in this work CO conversion changes in the range 15-75% have little influence on the product distribution over unpromoted and Cs-promoted Ru catalysts supported on high surface area graphite. Early results[56,57] on the effect of CO conversion level for Ru based catalysts supported on metal oxides reported changes in the product distribution. The authors reported a decrease for the chain termination probability and olefin content in the products with increasing bed residence time (increasing conversion level from 5 to 65 %). To explain these effects, a model based on readsorption and reinsertion processes of primary olefins is proposed.[56] However in our study, changes in product distribution would not be expected as all the catalysts were studied at similar space velocity (GHSV = 6.1 m^3_{STP} kg^{-1} h^{-1}).
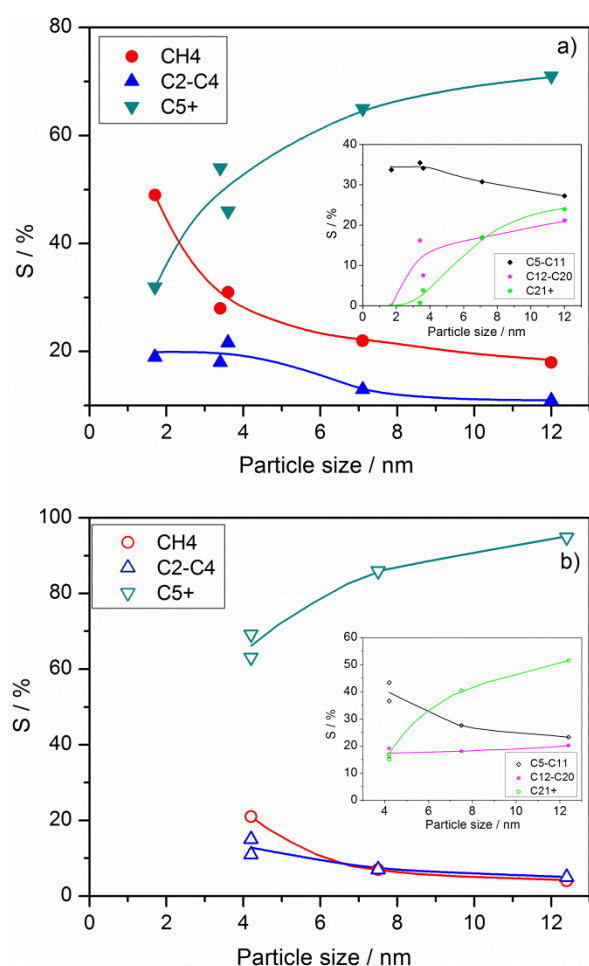
Figure 9. Effect of Ru particle size in FTS on selectivity towards different hydrocarbons for (a) unpromoted and (b) Cs-promoted catalysts. Inserts show the variation of C_5-C_{11}, C_{12}-C_{20} and C_{21+} selectivities with particle size.

Figure 9 shows that the product selectivity changes significantly with Ru particle size. Selectivities to CH_4 and C_2-C_4 clearly decrease with increasing Ru particle size from 1.7 to 7.1

nm and from 4.2 to 7.5 nm for unpromoted and promoted catalysts, respectively. A further increase in the Ru particle size to 12.0 nm (or 12.7 nm) slightly decreases the selectivities to these light hydrocarbons. Simultaneously, the selectivity to C_{5+} hydrocarbons, particularly that for C_{21+} (wax) (see insert in Figure 9) increases with Ru particle size. The high selectivity toward CH_4 (49%) obtained over the non-promoted Ru catalysts with the smallest particle size (1.7 nm) demonstrates that the presence of edges and sites with strong CO heat of adsorption results in very poor FTS performance. On the other hand, non-promoted catalysts with Ru particle size of 3.5 nm and above, and Cs-promoted catalyst with Ru particle size of 4.2 nm mainly produce hydrocarbons in the gasoline range (C_5-C_{11}), with a slight increase in the amount of C_{21+} for bigger particle sizes. However, over Cs-promoted catalysts with Ru particle sizes of 7.5 nm and above, C_{21+} hydrocarbons are much more abundant in the product. These results are in good agreement with FTS literature and particularly with results reported by Kang et al.[35] for Ru nanoparticles loaded on carbon nanotubes. They found that the selectivities to CH_4 and C_2-C_4 hydrocarbons decreased with increasing the size of the Ru nanoparticles, whereas that to C_{5+} hydrocarbons increased. It has been postulated that the higher C_{5+} selectivity of the larger Ru nanoparticles may be due to their higher active site densities, which may result in higher probability of re-adsorption and polymerization of α-olefin intermediates.[58]

Figure 10 depicts the effect of Ru particle size on the olefin to paraffin (O/P) ratio in the range of C_2-C_4 hydrocarbons. A continuous decline in the O/P ratio with the increasing size of the Ru particles for the non-promoted catalysts is observed, in agreement with the above speculation that on larger Ru particles the olefins are prone to re-adsorb and to be further hydrogenated. However, over Cs-promoted catalysts, the O/P ratio remains constant in the range of Ru particle size between 4.2-12.4 nm. It seems that for Cs-promoted catalysts the effect of the Cs promoter prevails over the Ru particle size effect. The presence of the promoter, as discussed above, hinders the hydrogen adsorption on the catalyst surface reducing the possibility to hydrogenate re-adsorbed olefins.
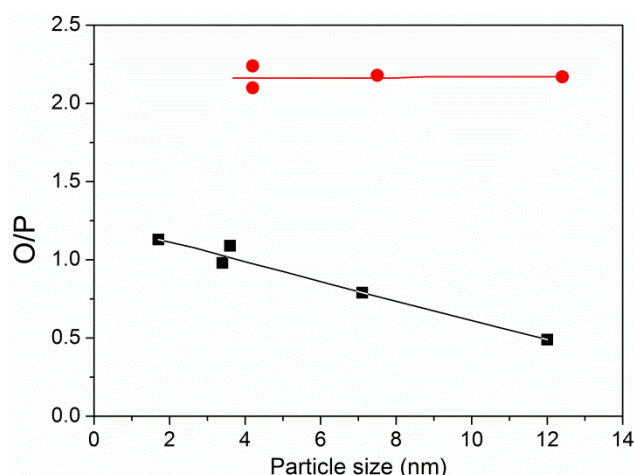
Figure 10. Effect of particle size on the olefins to paraffin ratio in the range of C_2-C_4 hydrocarbons for (■) unpromoted and (●) Cs promoted catalysts.

Conclusions

The influence of ruthenium particle size on the performance in FTS for Cs promoted and unpromoted high-surface-area-graphite supported catalysts has been studied. The use of a support with large surface area and weak interactions with Ru allows to independently study these effects without the influence of parasitic metal-support interactions. Microcalorimetric measurements of CO adsorption evidenced an increase in the heat of CO adsorption upon promoter addition. XPS demonstrates a clear interaction between Ru and Cs.

The TOF for CO conversion increases significantly with Ru particle size from 1.7 to 7.1 nm or 4.2 to 7.5 nm for unpromoted and promoted catalysts, respectively, and then change slightly up to 12 nm. The selectivity to C_{5+} hydrocarbons increases gradually with the Ru particle size for both series of catalysts. The O/P ratio over unpromoted catalysts decreases, whereas it remains constant over Cs promoted catalysts. Altogether, our results demonstrate the structure sensitive nature of FTS over Ru catalysts for Ru particles <7 nm, and highlight the great stability of these catalysts and the potential of Cs promotion for the preferential formation of waxes, even at high conversion levels.

Acknowledgements

Notes and references

1   Q. Zhang, J. Kang, V. Wang, *ChemCatChem.*, 2010, **2**, 1030.
2   H. Schulz, *Appl. Catal. A*, 1999, **186**, 3.
3   D. A. Simonetti, J. Rass-Hansen, E. L. Kunkes, R. R. Soares, J. A. Dumesic, *Green Chem.*, 2007, **9**, 1073.
4   T. E. Hoost, J. G. Goodwin Jr, *J. Catal.*, 1992, **137**, 22.
5   N. Lohitharn, J. G. Goodwin Jr, *J. Catal.*, 2008, **260**, 7.
6   M. C. Ribeiro, G. Jacobs, B. H. Davis, D. C. Cronauer, A. J. Kropf, C. L. Marshall, *J. Phys. Chem.*, 2010, **114**, 7895.
7   M. Guraya, S. Sprenger, W. Rarog-Pilecka, D. Szmigiel, Z. Kowalczyk, M. Muhler, *Appl. Surf. Sci.*, 2004, **238**, 77.
8   K. Aika, K. Shimazaki, Y. Hattori, A. Ohya, S. Ohshima, K. Shirota, A. Ozaki, *J. Catal.*, 1985, **92**, 296.
9   Z. Kowalczyk, M. Krukowski, W. Raróg-Pilecka, D. Szmigiel, J. Zielinski, *Appl. Catal. A*, 2003, **248**, 67.
10 J. L. Eslava, A. Iglesias-Juez, G. Agostini, M. Fernández-García, A. Guerrero-Ruiz, I. Rodríguez-Ramos, *ACS Catal.*, 2016, **6**, 1437.
11 S. L. Soled, E. Iglesia, R. A. Fiato, J. E. Baumgartner, H. Vroman, S. Miseo, *Top. Catal.*, 2003, **26**, 101.
12 S. Storsæter, B. Tøtdal, J. C. Walmsley, B. S. Tanem, A. Holmen, *J. Catal.*, 2005, **236**, 139.
13 J. L. Zhang, J. G. Chen, J. Ren, Y. W. Li, Y. H. Sun, *Fuel*, 2003, **82**, 581.
14 H. F. Xiong, Y. H. Zhang, S. G. Wang, J. L. Li, *Catal. Commun.*, 2005, **6**, 512.
15 D. C. Song, J. L. Li, *J. Mol. Catal. A*, 2006, **247**, 206.
16 H. F. Xiong, Y. H. Zhang, K. Y. Liew, J. L. Li, *J. Mol. Catal.* A, 2008, **295**, 68–76.
17 J. L. Li, G. Jacobs, Y. Q. Zhang, T. Das, B. H. Davis, *Appl. Catal. A*, 2002, **223**, 195.
18 G. L. Bezemer, J. H. Bitter, P. C. E. Kuipers, H. Oosterbeek, J. E. Holewijn, X. Xu, F. Kapteijn, A. J. van Dillen, K. P. de Jong, *J. Am. Chem. Soc.*, 2006, **128**, 3956.
19 J. C. Kang, S. L. Zhang, Q. H. Zhang, Y. Wang, *Angew. Chem. Int. Ed.*, 2009, **48**, 2565.
20 W. P. Ma, Y. J. Ding, L. W. Lin, *Ind. Eng. Chem. Res*., 2004, **43**, 2391.
21 K. Xiong, J. L. Li, K. Y. Liew, X. D. Zhan, *Appl. Catal. A*, 2010, **389**, 173.
22 L. Gonzalo-Chacón, M. Almohalla, E. Gallegos-Suarez, A. Guerrero-Ruiz, I. Rodríguez-Ramos, *Appl. Catal. A*, 2014, **480**, 86.
23 R. A. van Santen, *Acc. Chem. Res.*, 2009, **42**, 57.
24 D. Barkhuizen, E. I. Mabaso, E. Viljoen, C. Welker, M. Claeys, E. van Steen, J. C. Q. Fletcher, *Pure Appl. Chem.*, 2006, **78**, 1759.
25 G. Prieto, A. Martínez, P. Concepción, R. Moreno-Tost, *J. Catal.*, 2009, **266**, 129.
26 J. P. den Breejen, P. B. Radstake, G. L. Bezemer, J. H. Bitter, V. Frøseth, A. Holmen, K. P. de Jong, *J. Am. Chem. Soc.*, 2009, **131**, 7197.
27 A. Barbier, A. Tuel, I. Arcon, A. Kodre, G. A. Martin, *J. Catal.*, 2001, 200, 106.
28 R. C. Reuel, C. H. Bartholomew, *J. Catal.*, 1984, **85**, 78.
29 A. S. Lisitsyn, A. V. Golovin, V. L. Kuzketsov, Y. I. Yermakov, *J. Catal.*, 1985, **95**, 527.
30 J. Y. Park, Y. J. Lee, P. K. Khanna, K. W. Jun, J. W. Bae, Y. H. Kim, *J. Mol. Catal*. A, 2010, **323**, 84.
31 H. M. Torres-Galvis, J. H. Bitter, T. Davidian, M. Ruitenbeek, A. I. Dugulan, K. P. de Jong, *J. Am. Chem. Soc.*, 2012, **134**, 16207.
32 C. S. Kellner, A. T. Bell, *J. Catal.*, 1982, **75**, 251.
33 K. J. Smith, R. C. Everson, *J. Catal.*, 1986, **99**, 349.
34 E. Iglesia, S. L. Soled, R. A. Fiato, *J. Catal.*, 1992, **137**, 212.
35 J. Kang, W. Deng, Q. Zhang, Y. Wang, *J. Energy Chem.*, 2013, **22**, 321.
36 J. M. G. Carballo, J. Yang, A. Holmen, S. García-Rodríguez, S. Rojas, M. Ojeda, J. L. G. Fierro, *J. Catal.*, 2011, **284**, 102.
37 S. Shetty, R. A van Santen, *Catal. Today*, 2011, **171**, 168.
38 A. Guerrero-Ruiz, B. Bachiller-Baeza, I. Rodríguez-Ramos, *Appl. Catal. A*, 1998, **173**, 231-238.
39 J. R. Anderson, In Structure of Metallic Catalysts; Academic Press: London, 1975, pp 289-394.
40 P. Gallezot, C. Leclercq, in: B. Imelik, J. C. Vedrine, (Eds.), Physical Techniques for Solid Materials. Fundamental and Applied Catalysis, Plenum Press, New York, NY. 1994, p. 509.
41 S. Sartipi, K. Parashar, M. J. Valero-Romero, V. P. Santos, B. van der Linden, M. Makkee, F. Kapteijn, J. Gascon, *J. Catal.*, 2013, **305**, 179.
42 P. J. van de Brink, M. Bracht, G. J. M. Gruter, R. de Ruiter, B. H. Harji, Patent WO 02092220, 2002.
43 B. W. van Hasselt, H. P. A. Calis, S. T. Sie, C. M. van den Bleek, *Chem. Eng. Sci.*, 1999, **54**, 5047.
44 M. Cerro-Alarcón, A. Maroto-Valiente, I. Rodríguez-Ramos, A. Guerrero-Ruiz, *Carbon*, 2005, **43**, 2711.
45 A. Guerrero-Ruiz, P. Badenes, I. Rodríguez-Ramos, *Appl. Catal. A*, 1998, **173**, 313.
46 B. Bachiller-Baeza, A. Guerrero-Ruiz, P. Wang, I. Rodríguez-Ramos, *J. Catal.*, 2001, **204**, 450.
47 K. Lu, B. J. Tatarchuk, *J. Catal.*, 1987, **106**, 166.
48 E. Gallegos-Suarez, L. Gonzalo-Chacón, I. Rodríguez-Ramos, A. Guerrero-Ruiz, *Thermochim. Acta*, 2013, **567**, 112.
49 I. Rossetti, N. Pernicone, L. Forni, *Appl. Catal*. A, 2001, **208**, 271.
50 C. D. Wagner, W. M. Riggs, L. E. Davis, J. F. Moulder, G. E. Muilenberg, Handbook of X-Ray Photoelectron Spectroscopy, Perkin-Elmer Corp., Eden Prairie, Minnesota, 1979, p. 106.

51 D. Uzio, G. Berhault, *Catal. Rev.*, 2010, **52**, 106.
52 V. Ponec, G. C. Bond, Catalysis by Metals and Alloys, Elsevier, 1995, p. 239.
53 J. K. Nørskov, *Prog. Surf. Sci.*, 1991, **38**, 103.
54 R. A. van Santen, I. M. Ciobica, E. van Steen, M. M. Ghouri, *Adv. Catal.*, 2011, **54**, 127.
55 S. B. Vendelbo, M. Johansson, D. J. Mowbray, M. P. Andersson, F. Abild-Pedersen, J. H. Nielsen, J. K. Nørskov, I. Chorkendorff, *Top. Catal.*, 2010, **53**, 357.
56 E. Iglesia, S. C. Reyes, R. J. Madon, *J. Catal.*, 1991, **129**, 238.
57 J. Yang, W. Ma, D. Chen, A. Holmen, B. H. Davis, *Appl. Catal. A*, 2014, **470**, 250.
58 E. Iglesia, *Appl Catal. A*, 1997, **161**, 59.